Journal of Alloys and Compounds 509 (2011) 5581–5586

Contents lists available at ScienceDirect

Journal of Alloys and Compounds

journal homepage: www.elsevier.com/locate/jallcom

Preparation of Fe-based monodisperse spherical particles with fully glassy phase

Ayako Miura*, Wei Dong[1], Masahiro Fukue, Noriharu Yodoshi, Kenta Takagi[2], Akira Kawasaki

Department of Materials Processing, Graduate School of Engineering, Tohoku University, 6-6-02 Aoba, Aramaki, Aobaku, Sendai 980-8579, Japan

ARTICLE INFO

Article history:
Received 29 October 2010
Accepted 7 February 2011
Available online 1 March 2011

Keywords:
Metallic glasses
Amorphous materials
Microstructure
Rapid-solidification
Powder metallurgy

ABSTRACT

In this study, we prepared monodisperse spherical particles of a desired diameter using $[(Fe_{0.5}Co_{0.5})_{0.75}B_{0.2}Si_{0.05}]_{96}Nb_4$ alloy; the particles were prepared by using an atomization process developed by us. The particles have perfect sphericity and narrow size distribution along with a homogeneous composition. The phase transitions of particles from the fully glassy phase to the crystalline phase via mixed phase structures occurred as the particle diameter was increased; the particles produced in the fully glassy phase in an argon atmosphere had a diameter of less than 300 μm. This allowed the estimation of the intrinsic critical cooling rate for the particles with a fully glassy phase, R_c:R_c varied in the range of 700–900 K/s and depended only on the initial temperature of the alloy melt.

1. Introduction

Fe-based metallic glass has attracted considerable attention as a potentially practical amorphous material because it has various desirable properties as well as cost advantages. Numerous researches have demonstrated that the Fe-based metallic glass possesses high strength and excellent soft magnetic properties [1,2]. In particular, the composition of $[(Fe_{0.5}Co_{0.5})_{0.75}B_{0.2}Si_{0.05}]_{96}Nb_4$ alloy makes it more suitable to be used for producing glass than other Fe-based compositions [2,3]. This composition, however, requires a high cooling rate of over 10^3 K/s for the formation of the glassy phase as compared to the cooling rate required by other typical metallic glasses, because the thermal stabilities of this alloy are comparatively less than Zr- and Pd-based alloys [4]. Thus, conventional glass-forming techniques such as melt spinning and casting are unsuitable for producing practically large quantities of the Fe-based metallic glass because of size limitations and a lack of quenching capability. Therefore, the fabrication of Fe-based metallic glasses has been recently attempted by using powder metallurgic approaches. Typically, a metallic glass powder is prepared and then consolidated for bulk formation by hot compressing or spray forming [5,6]. These approaches are expected to achieve not only bulk formation but also a near net shape.

So far, gas atomization and spraying processes have been used to prepare the metallic glass powders [5–8]. These mature powdering processes can easily produce powders of any metal in large quantities. The powders produced, however, are fairly polydispersed; consequently, the individual particles inevitably solidify under different cooling conditions such as flight velocity, trajectory, droplet size, and atmosphere temperature. Thus, it is very difficult to ensure full glassification in the polydispersed powder. In addition, the unintended polydispersity is not suitable for the subsequent consolidation process. To prevent crystallization, the consolidation of metallic glass powder is based only on the powder compacting process within a viscous flow deformation of particles [9], whereas the consolidation of a common glass powder also involves sintering. In general, most of the metallic glasses, particularly the Fe-based ones, show a viscous flow behavior in a narrow temperature range, i.e., in the narrow undercooled liquid region, in which the sensitivity of viscous flow deformation is widely known [10,11]. Thus, it is feared that long heating and fluctuation of temperature during the process could cause crystallization. One effective method to obtain high-quality and dense bulk metallic glasses is to carry out densification using a glassy powder whose size can be precisely controlled; the use of a powder whose particle size distribution can be controlled will improve the densification process dramatically owing to dense packing.

From this point of view, we propose the preparation of monodisperse spherical particles of Fe-based metallic glass. Hitherto, we

* Corresponding author. Present address: Steel Research Laboratory, JFE Steel Corporation, 1, Kawasaki-cho, Chuo-ku, Chiba 260-0835, Japan.
Tel.: +81 43 262 2918; fax: +81 43 262 4730.
E-mail addresses: a-miura@jfe-steel.co.jp (A. Miura), w-dong@dult.edu.cn (W. Dong), a9tm5625@stu.material.tohoku.ac.jp (M. Fukue), ynoriharu@material.tohoku.ac.jp (N. Yodoshi), k-takagi@aist.go.jp (K. Takagi), kawasaki@material.tohoku.ac.jp (A. Kawasaki).
[1] Present address: School of Material Science and Engineering, Dalian University of Technology, No. 2 Linggong Road, Ganjingzi District, Dalian City, Liaoning Province 116024, China.
[2] Present address: National Institute of Advanced Industrial Science and Technology, 2266-98 Shimo-Shidami, Moriyamaku, Nagoya 463-8560, Japan.

0925-8388/$ – see front matter © 2011 Elsevier B.V. All rights reserved.
doi:10.1016/j.jallcom.2011.02.044

have successfully developed a unique atomization process which is capable of producing monodisperse particles of various materials, by a method called the pulsated orifice ejection method (POEM) [12,13]. The POEM is able to mass-produce monodisperse particles of the desired diameter in the range of several tens to hundreds of micrometers. Furthermore, the prepared particles have a narrow size less than 2% of the standard deviation unit. The capability to control the size and the monodispersity allow effective densification of powders as mentioned above. In addition, the monodisperse powders formed by this method completely undergo the same cooling procedure. This means that all the particles completely repeat the identical cooling and solidification processes. Therefore, the preparation of monodisperse particles facilitates the understanding of the solidification behavior and consequently the preparation of high-quality metallic glass particles.

This study aims to prepare monodisperse $[(Fe_{0.5}Co_{0.5})_{0.75}B_{0.2}Si_{0.05}]_{96}Nb_4$ metallic glass alloy particles with a narrow size distribution and a homogeneous glassy phase structure by the POEM. We also discuss the direction of approach of preparing a high-quality metallic glass powder, based on the fundamental study of the mechanism of glass phase formation during container-less solidification.

2. Material and methods

Raw alloy ingots with a composition of $[(Fe_{0.5}Co_{0.5})_{0.75}B_{0.2}Si_{0.05}]_{96}Nb_4$ were prepared by induction melting from the following constituent materials: 99.9% cobalt blocks, 99.99% iron granules, 99.5% boron granules, 99.999% silicon granules and 99.9% niobium granules (all were manufactured by Japan Pure Chemical Co. Ltd., Japan). The starting materials were remelted in an argon atmosphere to avoid oxidation.

Meanwhile, the POEM forms monodisperese particles through three steps: ejection of a molten droplet downward from an orifice in the bottom of a crucible by a pulsated mechanical pressure, spontaneous spheronization of the falling droplet, and container-less solidification. The repetition of this sequence at a quick rate enables the mass-production of monodisperse particles. The details of the POEM have been described in previous studies [12,13].

A first touchstone in this study was to stably form the monodisperse droplets of $[(Fe_{0.5}Co_{0.5})_{0.75}B_{0.2}Si_{0.05}]_{96}Nb_4$ alloy. Selecting material for the parts that are directly exposed to the molten alloy was the most important factor to achieve stable ejection and purity of droplets. Our previous studies have shown that the ejection of droplets is mainly governed by the wettability of the molten raw material to the orifice surface [12]. Hence, the contact angles of the alloy to boron nitride and alumina, which were chosen as the ceramic candidates for the orifice, were measured by a sessile drop method in an argon atmosphere. As a result, both the ceramics had adequately high contact angles of around 120–160° above 1493 K (the melting point of the raw material). We adopted boron nitride as the material for the orifice and crucible because of its workability. Only the rod, which played the role of propagating the pulsated pressure to the melt, was made of alumina, because of its high temperature strength.

Crushed pieces of the raw alloy were put in the crucible, the orifice of which had a 400 μm-diameter. The rod and the crucible containing the raw alloy were set up on the ejection device, which was fitted on the top of a drop-tube in the POEM apparatus. One end of the rod was interlocked with a piezoelectric actuator in the ejection device, and the other end was positioned at 0.9 mm from the orifice. The sealed crucible and tube were purged with high-pure argon gas (>99.9995%), and then the crucible was heated up to 1473 and 1523 K by a tungsten resistance heating.

To eject the droplets, pulsated pressure was applied to the melt near the orifice by a vertically reciprocating action of the rod at a frequency of 10 Hz. The downward and upward velocities of the rod motion and the rod displacement can be precisely controlled by a voltage waveform applied to the piezoelectric actuator. Constant gas pressure was also applied to the molten alloy to assist the droplet ejection. Actually, the particles were prepared by varying the process parameters of the rod displacement, downward velocity of the rod, and assistant gas pressure.

The size and geometry of the prepared particles were measured using an optical microscope coupled to an image analyzer. The surface morphology and cross-sectional microstructure of the particles were observed by a scanning electron microscope (SEM: JSM-6060, JEOL Co. Ltd., Japan). To identify the microstructure, the polished cross-sections were chemically etched using a mixture of 100 ml ethanol and 6 ml nitric acid (HNO_3) (1.38 M). The crystal structures of the particles were identified by X-ray diffraction (RINT-2400, Rigaku Co. Ltd., Japan) with CuKα. Thermal stabilities including glass transition temperature T_g, crystallization temperature T_x and supercooled liquid region $\Delta T_x = T_x - T_g$ were determined by differential scanning calorimetry (DSC: DSC 6300, Seiko Instruments Inc., Japan) at a heating rate of 0.67 K/s under pure argon atmosphere. The detailed microstructure and composition of the particles was also observed by a field emission transmission electron microscope coupled by energy dispersive X-ray spectroscope (TEM-EDX: HF-2000, Hitachi Ltd., Japan). The TEM specimens were polished by an ion milling.

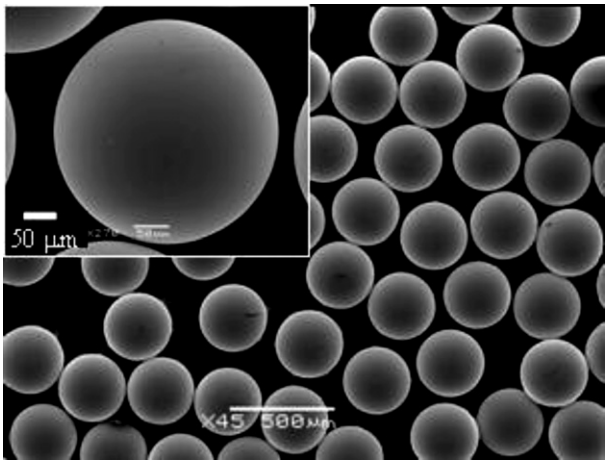

Fig. 1. SEM images of particles with diameter of 311 μm.

3. Results

Monodisperse spherical particles with a diameter of 70–100% of the orifice diameter were successfully prepared by adjusting the process parameters. Fig. 1 shows a typical SEM image of the particles prepared in this study. These particles had particularly smooth surfaces compared to the crystalline metal particles that had ever been obtained by atomization including the POEM. The crystalline particles have more or less a rough surface texture due to grain boundaries and preferred growth orientation [12,13], but the present particles showed no crystalline vestige. In the case of the indicated particles, the average diameter, the size distribution, and the sphericity were determined to be 311 μm, 1.24 μm, and 1.57%, respectively. The other groups of particles obtained also showed a very smooth surface, high monodispersity, and similar sphericity.

Fig. 2 shows the relationships between the process parameters and the particle size. The particle diameter was found to be almost linearly dependent on the two process parameters: assistant gas pressure and rod displacement. The downward velocity also seemed to be a dominant parameter affecting the diameter. This result indicated that adjusting these process parameters allows us to precisely control the diameter in a wide range as expected. In addition, the precise size controllability will help to prepare high-quality glass particles, because the droplet size would be dominant of the cooling rate of the droplets, namely glassy phase formation in the particles [5,6,9].

Fig. 3 shows the X-ray diffraction patterns for some of the particles obtained corresponding to Fig. 2(b). The largest particles (particle A) with the diameter of 390 μm clearly showed the crystalline peaks. However, the peaks became ambiguous gradually as the particle size was reduced, and eventually the particle of 291 μm (particle F) showed only the broad peaks. The result implied that the volume of the glassy phase increased with the reduction in particle size.

Fig. 4 shows the TEM bright field image and the selected-area electron diffraction pattern in the central region of the particle F, which showed the broadest diffraction pattern in Fig. 3. The obvious crystal structure was not found in this bright field image, and the halo pattern emerged in the electron diffraction pattern. Thus, the center region certainly consisted of a single glassy phase. Forming the glassy phase was supposed to be most difficult in the central region, because this region would not benefit much by the rapid

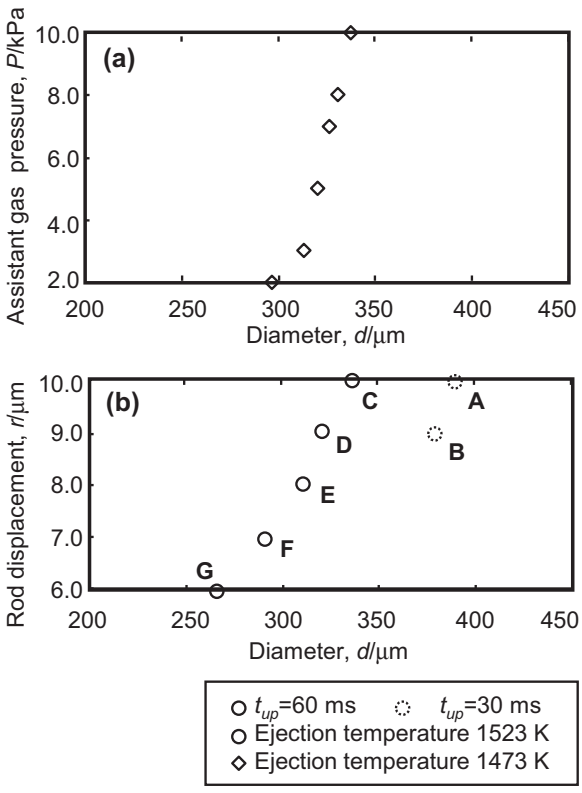

Fig. 2. Diameter of obtained particles (a) in relation to assistant gas pressure (P) (r = 8.0 μm at 1473 K) and (b) in relation to rod displacement (r) and t_{up} (P = 8.0 kPa at 1523 K).

cooling due to the heat transfer between the particle surface and the gas atmosphere. Furthermore, the entire particle F was estimated to consist of the glassy phase. On the other hand, Fig. 5 indicates the SEM image of a cross-section of the particle A, which was the largest particle showing the crystalline peaks in its X-ray diffraction pattern. The particle showed white and gray areas, which were identified as the crystalline and glassy phases by the TEM electron diffraction patterns. Most of the crystalline phases were embedded

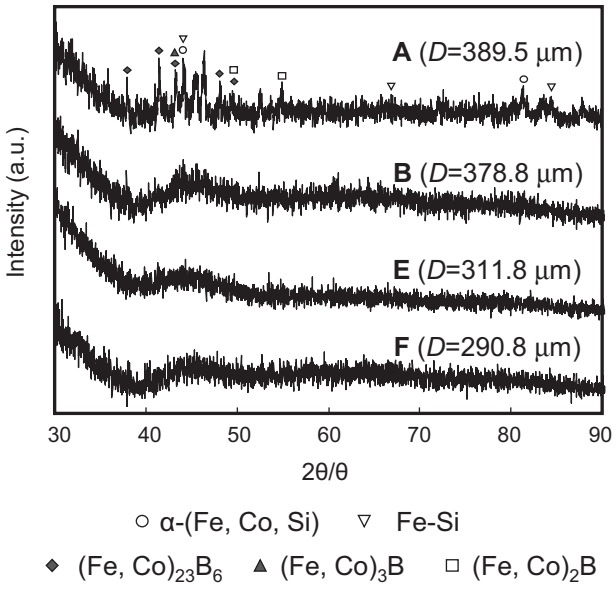

Fig. 3. X-ray diffraction patterns of monodisperse particles with various diameters prepared by POEM marked by A, B, E, and F in Fig. 2.

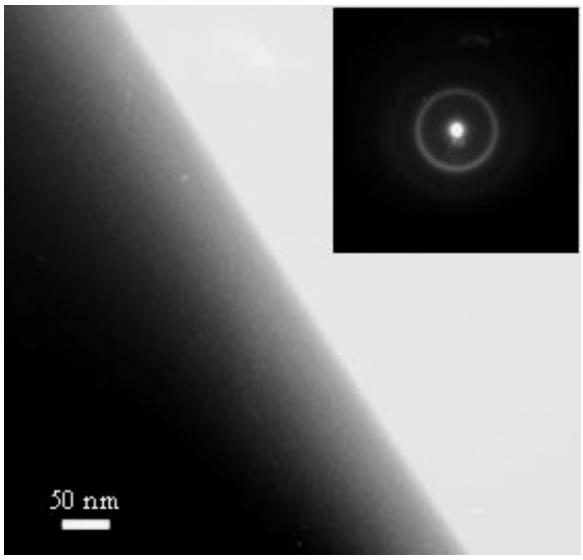

Fig. 4. TEM bright field image and SAED pattern at center part of fully glassy phase particle marked by F in Fig. 2.

with a circular shape into the glassy phase matrix, although some emerged at the surface region. Hence, the crystalline phases were dispersed all over the particle, implying an occurrence of statistical homogeneous nucleation. Furthermore, the TEM-EDX analyses, for the sample particle A in Fig. 5, showed that the composition of the crystalline phases was almost the same as that of the glassy phases, and it supported the idea that segregation was not the cause of crystallization in the POEM particles. From these results, it can be inferred that the nucleation supposedly occurred because the reduction in the cooling rate, which depends on the particle size.

The glassy fraction of the particles formed through containerless solidification was presumed to increase as the particle size reduced, and attain full occupancy below a certain particle size. So far, some researchers have successfully demonstrated the relationship between the volume of the glassy phase and the size of the rod-shaped sample for various compositions by a thermally analytical approach [1,14]. Fig. 6 shows the result of the DSC analysis for the particles indicated in Fig. 3. As the temperature increased, all

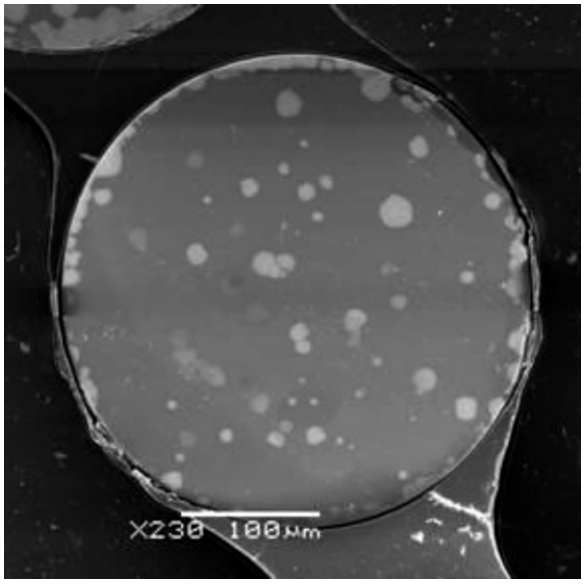

Fig. 5. SEM image of cross section of mixed phase particles marked by A in Fig. 2.

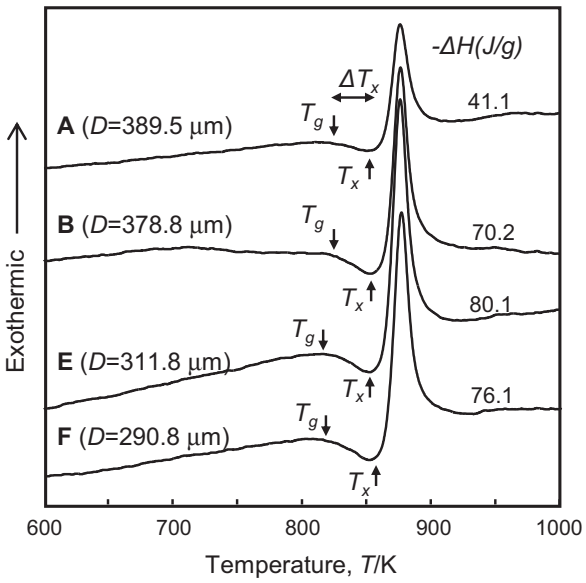

Fig. 6. DSC curves of monodisperse particles with various diameters prepared by POEM marked by F in Fig. 2.

the types of particles exhibited a decrease in the exothermic heat from around 830 K due to the glass transition. This was followed by the sharp exothermic peak derived from the crystallization after a supercooled liquid region. However, careful comparison of these particles confirmed that the enthalpy for crystallization and the range of the supercooled liquid region were likely to increase as the particle size reduced. These changes indicated the possibility of estimating the glassy phase fraction quantitatively [15]. Fig. 7 shows the calculated glassy fraction as a function of the diameter of the particle. The glassy fractions were determined as the ratio of each enthalpy ΔH to the enthalpy of the fully glassy phase particle ΔH_{glass}. In this study, particle F was assumed to be the fully glassy particle in keeping with the evidence mentioned above. The diameter of the emerging crystalline phases, i.e., transition diameter was obviously larger than 300 μm. The previous researches have estimated that the diameter of the particle ranged between 200 μm in the transition region from fully glassy to crystalline [16,17], but in our research, it appeared within 100 μm. This is because the monodispersity of the POEM particles was more accurately obtainable in the transition region, and it was advantageous to estimate the critical cooling rate strictly.

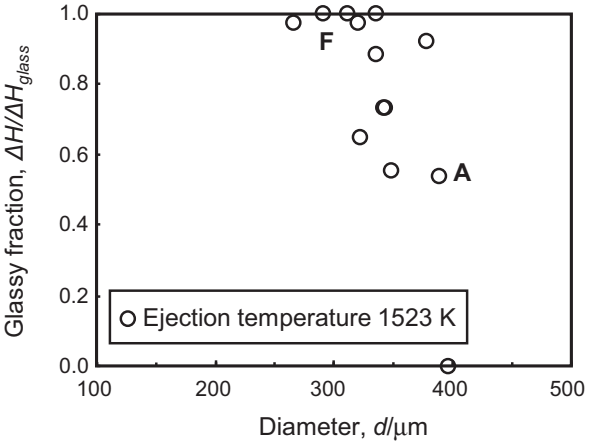

Fig. 7. Glassy fraction of particles as a function of particle diameter.

From these results, monodisperse fully metallic glass particles of the desired size were successfully prepared by the POEM. In addition, this achievement offered the possibility to estimate intrinsic critical cooling rate of this alloy.

4. Discussion

In general, the formation of metallic glasses is discussed along with the cooling process of the liquid alloy passing through its glass transition temperature, and it is unexceptional in the case of droplets. As a matter of fact, the container-less solidification of droplets offers an ideal situation for glass formation in terms of no nucleation site and small temperature distribution, which has often been realized by static floating techniques. However, in the case of atomization processing, it has been extremely difficult to monitor or estimate the thermal profile of individual droplets. On the other hand, the POEM forms all the droplets with the same volume and they fall on an identical trajectory with an identical velocity. Thus, the cooling rate of the droplets must be estimated fairly exactly.

A droplet falling in static atmosphere gas is assumed as a static droplet undergoing gas flow. The gas flow rate, thus, is defined to be equal to the droplet falling velocity. The temperature of droplet T at time t is expressed as follows.

$$T = T_a - (T_a - T_0)e^{-mt} \tag{4.1}$$

with

$$m = \frac{hS}{\rho C_P V} \tag{4.2}$$

where, T_0 and T_a represent the initial temperature of the droplet and the atmospheric temperature, S and V are the surface area and volume of the droplet. ρ and C_p are the density and the specific heat of the droplet, h is the heat transfer coefficient under forced convection flow, and can be calculated by the Ranz–Marshall equation [18]:

$$Re < 1000 : Nu = 2.0 + 0.6Re^{1/2} \cdot Pr^{1/3} \tag{4.3}$$

where

$$Nu = \frac{hd}{\lambda}, \quad Re = \frac{du}{\nu} \text{ and } Pr = \frac{\nu}{\alpha} \tag{4.4}$$

here, Nu, Pr, and Re are the Nusselt, Prandtl, and Reynolds number, respectively; d and u represent the droplet diameter and the gas flow rate, i.e., the droplet falling velocity, respectively; and λ, ν, and α are the thermal conductivity of the gas, kinetic viscosity of the gas, and thermal diffusivity, respectively. The details of the formulae have been explained in our previous study [13]. In the case of amorphous structure alloys, atomic movement becomes slower below the temperature of the liquid and then is frozen at the glass transition temperature [19]. Thus, we tried to calculate the mean cooling rate in the temperature range from T_l to T_g. The cooling rate R was obtained following:

$$R = \frac{T_l - T_g}{\Delta t} \tag{4.5}$$

here, Δt is the time to chill from T_l to T_g, which can be calculated by Eqs. (4.1)–(4.5).

Fig. 8 shows the relationships between the calculated cooling rate the diameter and the glassy quality for all the particles obtained in this study. The thermophysical properties of the gases and droplets in Table 1 were used to calculate the cooling rates [20–22]. The atmospheric temperature T_a and the droplet falling velocity u were experimentally acquired by a temperature distribution measurement with thermocouples and a high-speed camera observation, respectively. The glassy qualities were classified into the following three levels based on the results of thermal analysis: fully glassy, glass mixed, and fully crystalline particles. As a result

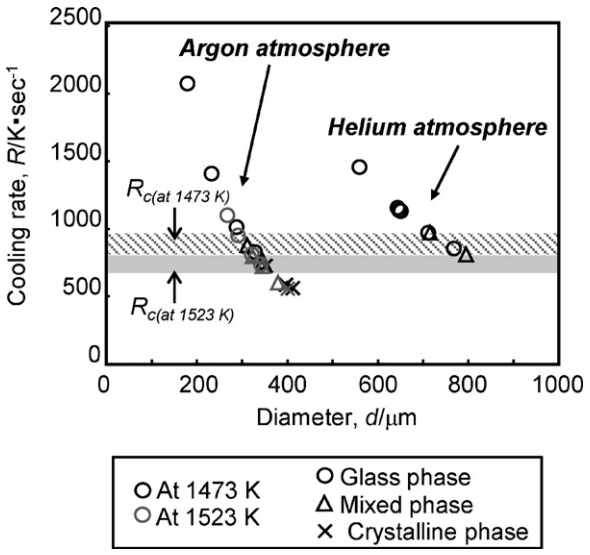

Fig. 8. Relationship between cooling rates of particles prepared by POEM in argon (at 1473 and 1523 K) or helium atmosphere (at 1473 K), their structures as a function of particle diameters, and their critical cooling rates. (R_c represents the critical cooling rate.).

of the calculations, the change in the diameter was estimated to yield a large difference in the cooling rate. For example, the cooling rate quadruples when the particle size is reduced to half. The result of this calculation is a convincing proof of the microstructural transition depending on the cooling rate. Indeed, Fig. 8 shows the continuous changes in the glassy quality from the fully crystalline phase to the fully glass phase, with an increasing cooling rate. The critical cooling rate R_c for forming the fully glass phase was definitely determined to be 700–900 K/s from Fig. 8. This value was less than 10^3 K/s, which has been reported as the critical cooling rate estimated using the cast Fe-based bulk metallic glass [23]. This implies that heterogeneous nucleations were suppressed in the POEM because of container-less solidification [13]. Thus, R_c was considered to be the intrinsic critical cooling rate of this Fe-based metallic glass.

Let us discuss this result in further detail. Solidification of metallic glass is a unique phenomenon as has been reported previously [7,15–17,19]. Basically, the atom configuration in melt of metallic glass is dense and random according to Inoue's three rules, and is frozen without reconstruction to the crystalline phase during quenching. Thus, the atomic configuration in melt is supposed to reflect that after solidification [15,16]. Furthermore, the crystalline phase appearance was supposed to start from particular atomic bindings in the melt, such as quenched nuclei, intermetallic compound, and so on [24,25]. However, the previous reports have suggested that the atomic configuration including the atomic bindings changed with the degree of superheating [26–28].

In Fig. 8, when the initial temperature changed from 1473 K to 1523 K, the critical cooling rate moved to the lower range of 550–700 K/s. This phenomenon may be related to the atomic movement in the melt. If so, the higher initial temperature brings a more random atomic configuration, and as a result reduces R_c. On the other hand, in the lower initial temperature, more atomic bindings would exist as written before [24,25]. The atom configuration in the largely overheated melt is more random [26–28]. Possibly, this marked random amorphous structure is maintained after quenching [15,17,29]. On the contrary, if the overheating is not large, a certain kind of atom binding easily remains in the melts. These bindings originate at latent nucleation sites for solidification [24,25]. It means, the change in R_c at the initial temperature could be explained by considering the atomic configuration.

Meanwhile, when the cooling media changed from argon gas to helium gas, the critical cooling rate did not change. As a result, changing the cooling media changed the critical particle size for the fully glassy phase, but eventually it would not affect the critical cooling rate. In other words, at a fixed initial temperature, the occurrence of the crystalline phase depends only on cooling rates, during solidification.

Table 1
Thermophysical properties of gases and droplets used for calculation.

Symbol	Nomenclature	Value (Ar/He)	Reference
λ_g	Thermal conductivity (W/(m K))	$1.763 \times 10^{-2}/15.27 \times 10^{-2}$	[20]
ρ_g	Density (kg/m^3)	1.624/0.162	[20]
n_g	Kinematic viscosity (m^2/s)	$13.99 \times 10^{-6}/122.0 \times 10^{-6}$	[20]
C_p	Specific heat (J/(g K))	0.5215/5.193	[20]
T_l	Liquidus temperature (K)	1431	[1]
τ_g	Glass transition temperature (K)	820	[1]
ρ_l	Density (kg/m^3)	7710	[21]
C_P	Specific heat (J/(g K))	0.7423	[21,22]

5. Conclusions

Monodisperse $[(Fe_{0.5}Co_{0.5})_{0.75}B_{0.2}Si_{0.05}]_{96}Nb_4$ metallic glass alloy particles with a high sphericity were successfully prepared by the POEM. The results of structural and thermal analyses showed that the prepared particles exhibited a homogeneous glassy phase. In addition, the microstructure of the particles changed from a fully crystalline phase to a fully glassy phase with a reduction in the size of the particle. The calculation of the droplet temperature revealed that this transition was caused only by the change in the cooling rate of the falling alloy droplets. In addition, the experiment using the POEM could be used to determine the critical cooling rate with relative accuracy due to the size monodispersity. Furthermore, the critical cooling rate changed depending on the initial temperature of the melt because of its particular atomic configuration. In addition, the critical cooling rate of this alloy was 700–900 K/s, which was lower than the lowest value that has been estimated using ribbon or casting techniques so far (10^3 K/s). Such estimation will facilitate the preparation of high-quality metallic glass particles with a homogeneously glassy phase, monodisperse and spherical shape stably; such powders can be used in powder metallurgical processes.

References

[1] A. Inoue, B.L. Shen, C.T. Chang, Acta Mater. 52 (2004) 4093–4099.
[2] A. Inoue, B. Shen, Mater. Trans. 43 (2002) 766–769.
[3] A. Inoue, Acta Mater. 48 (2000) 279–306.
[4] J. Pan, Q. Chen, N. Li, L. Liu, J. Alloy Compd. 463 (2008) 246–249.
[5] C.R.M. Afonso, C. Bolfarini, W.J. Botta Filho, C.S. Kiminami, Mater. Sci. Eng. A449–451 (2007) 884–889.
[6] M.L.T. Guo, C.Y.A. Tsao, J.C. Huang, J.S.C. Jamg, Mater. Sci. Eng. A404 (2005) 49–56.
[7] D.M. Herlach, Mater. Sci. Eng. R12 (1994) 177–272.
[8] S. Venkataraman, S. Scudino, J. Eckert, T. Gemming, C. Mickel, L. Schultz, D.J. Sordelet, J. Mater. Res. 21 (2006) 597–607.
[9] J. Kim, S. Yoon, H. Choi, H. Kim, H. Jo, C. Lee, Rev. Adv. Mater. Sci. 18 (2008) 46–49.
[10] Y. Kawamura, T. Itoi, T. Nakamura, A. Inoue, Mater. Sci. Eng. A304–306 (2001) 735–739.
[11] G. Wang, J. Shen, J.F. Sun, Y.J. Huang, J. Zou, Z.P. Lu, Z.H. Stachurski, B.D. Zhou, J. Non-Crystal. Solid 351 (2005) 209–217.
[12] K. Takagi, S. Masuda, H. Suzuki, A. Kawasaki, Mater. Trans. 47 (2006) 1–6.
[13] S. Masuda, K. Takagi, W. Dong, K. Yamanaka, A. Kawasaki, J. Crystal Growth 310 (2008) 2022–2915.
[14] F. Jiang, Z.B. Zhang, L. He, J. Sun, H. Zhang, Z.F. Zhang, J. Mater. Res. 21 (2006) 2638–2645.
[15] G. Li, Y.P. Gao, Z.H. Chi, R.P. Liu, J. Alloy Compd. 433 (2007) 233–236.
[16] F. Gillessen, D.M. Herlach, Mater. Sci. Eng. 97 (1988) 147–151.

[17] A. Dunst, D.M. Herlach, F. Gillessen, Mater. Sci. Eng. A133 (1991) 785–789.
[18] W.E. Ranz, W.R. Marshall, Chem. Eng. Prog. 48 (1952) 141–146.
[19] H.S. Chen, Rep. Prof. Phys. 43 (1980) 353–432.
[20] Netsubusseigakkai, Thermophysical Properties Handbook, Youkendou, Tokyo, 2000.
[21] The Japan Institute of Metal, Kinzoku Data Book, vol.3, Maruzen Co. Ltd., Tokyo, 1993.
[22] P.–F. Paradis, T. Ishikawa, S. Yoda, J. Mater. Sci. 36 (2001) 5125–5130.
[23] N. Yodoshi, R. Yamada, A. Kawasaki, R. Watanabe, Mater. Trans. 50 (2009) 2264–2269.
[24] A. Gupta, M.E. Jayaraj, S. Lal, R.P. Berma, J. Phys. F: Met. Phys. 18 (1988) 2159–2169.
[25] D.M. Herlach, F. Gillessesen, J. Phys. F: Met. Phys. 17 (1987) 1635–1644.
[26] K.F. Kelton, Intermetallics 14 (2006) 966–971.
[27] T. Heumann, Diffusion in Metallen, Springer, Tokyo, Japan, 2005.
[28] J.W.P. Schmelzer, J. Non-Cryst. Solids 354 (2008) 269–278.
[29] D.R. Allen, J.C. Foley, J.H. Perepezko, Acta Mater. 46 (1998) 431–440.